2.19

ATOMISTIC CALCULATION OF MECHANICAL BEHAVIOR

Ju Li

Department of Materials Science and Engineering,
Ohio State University, Columbus, OH, USA

Mechanical behavior is stress-related behavior. This can mean the material response is driven by externally applied stress (or partially), or the underlying processes are mediated by an internal stress field; very often both are true. Due to defects and their collective behavior [1], the spatiotemporal spectrum of stress field in a real material tends to have very large spectral width, with non-trivial coupling between different scales, which is another way of saying that the mechanical behavior of real materials tends to be multiscale. The concept of stress field is usually valid when coarse-grained above a few nm; in favorable circumstances like when crystalline order is preserved locally, it may be applicable down to sub-nm lengthscale [2]. But overall, the atomic scale is where the stress concept breaks down, and atomistic simulations [3–5] provide very important termination or matching condition for stress-based theories. Large-scale atomistic simulations (Chap. 2.25) are approaching μm lengthscale and are starting to reveal the collective behavior of defects [6]. But studying defect unit processes is still a main task of atomistic simulation.

It is infeasible to list the current developments in this area to any degree of completeness, so only a few highlights are given. A somewhat more detailed review can be found in Ref. [5].

- The study of deformation [7–11], grain growth [12] and fracture [13, 14] in nanocrystalline materials.
- Atomistic simulation of adhesion and friction [15, 16], and nanoindentation [17–20].
- The study of dislocation core structure and Peierls stress in BCC metals [21], semiconductors [22] and intermetallics [23]. A proper definition of dislocation core energy and numerically precise ways [24, 25] to extract

the core energy from periodic boundary condition (PBC) atomistic calculations.

- Thin film deposition, texture evolution and mechanical properties [26, 27].
- The study of dynamical brittle fracture [28, 29] and lattice trapping barriers [30, 31, 2], ductile fracture [6, 32].
- The study of phase and grain boundaries [33, 34].
- Deformation and fracture of amorphous materials [35].
- The application of Hessian-free minimum energy path (MEP) search algorithms [36] to study dislocation cross-slip in FCC metals [37], double kink nucleation and migration in semiconductors [38] and BCC metals [39], and heterogeneous dislocation nucleation at crack tips [2].
- Defect generation/evolution induced by irradiation, and effect on mechanical properties [40–42].
- Connection of atomistics to the mesoscale [43–46].

In this contribution, we review the basic concepts of strain, stress and elastic constant [47]. Then we move to a discussion about dislocation core energy [25]. Finally we discuss a minimum energy path calculation of heterogeneous dislocation nucleation at an atomically sharp crack tip [2].

1.   Strain, Stress and Elastic Constants

Stress and strain have many definitions, which although do not change the physics, differ in the efficiency of representing a particular problem. Here we introduce a system that is usually the most convenient for atomistic calculations.

Strain should be *relative*. To define strain, one must first declare the reference state. This is reasonable because strain describes deformation. Strain should be frame-covariant like any true second-rank tensor [48], since how much an object is deformed does not really depend on the angle one looks at it. Here we denote the geometrical configuration of an object by X, Y or Z, which describes its shape, i.e., surface constraints. For periodic boundary condition (PBC) simulations, this would be the supercell H-matrix (Chap. 2.8).

Affine transformation of an object from one shape to the other is specified by the tensor J, expressed as $Y = JX$, which is homogeneous in the sense that surface constraints of the object change uniformly according to J. But it does not have to be a microscopically homogeneous transformation, as different kinds of atoms may have different atomic-scale relaxations.

The Lagrangian strain is defined to be,

$$\eta_X^Y \equiv \tfrac{1}{2}(J^T J - 1). \tag{1}$$

Subscript X in η_X^Y denotes the reference state and superscript Y denotes the final state. If the final state is apparent we may omit the superscript and simply write as η_X.

The polar decomposition theorem [49] states that every matrix can be uniquely expressed as the left or right product of a symmetric matrix and a rotational matrix,

$$\begin{cases} J = RM = ML \\ M^T = M, R^T R = L^T L = 1 \end{cases} \tag{2}$$

Therefore,

$$\eta_X = \tfrac{1}{2}(J^T J - 1) = \tfrac{1}{2}(M^2 - 1). \tag{3}$$

There is one-to-one correspondence between η_X and M, as,

$$M = \sqrt{1 + 2\eta_X} = 1 + \eta_X - \tfrac{1}{2}\eta_X^2 + \dots \tag{4}$$

Let $Y = JX$, $Z = KY = KJX$. There is

$$\begin{aligned} \eta_Y^Z &= \tfrac{1}{2}(K^T K - 1), \\ \eta_X^Z &= \tfrac{1}{2}(J^T K^T K J - 1) \\ &= \tfrac{1}{2}(J^T(1 + 2\eta_Y^Z)J - 1) \\ &= J^T \eta_Y^Z J + \eta_X^Y, \end{aligned} \tag{5}$$

which is the law of η conversion between reference systems.

Contrary to strain, stress should be *absolute*, meaning it should not depend on any reference state besides the current state of the object. We use two definitions of stress here: the first is the external stress τ_{ij}, which is the usual "force per area" definition used by engineers,

$$dT_i = \tau_{ij} n_j \, dS, \tag{6}$$

where dT_i is the external traction force, n_j is the outward surface normal and dS is the surface area, and the Einstein summation convention is used. τ_{ij} is what the outside environment exerts on the object. To prevent rotation, it must satisfy $\tau_{ij} = \tau_{ji}$.

The second kind of stress is the thermodynamic stress t_{ij}, also called the intrinsic stress of the material volume, whose definition is based on the Helmholtz free energy $F(N, T, X)$ of the object:

$$F(N, T, X) = E - TS \equiv -k_B T \ln Z(N, T, X) \tag{7}$$

where $Z(N, T, X)$ is the partition function [50, 51],

$$Z(N, T, X) \equiv \int_X \exp(-\beta \mathcal{H}(q^N, p^N)) \frac{dq^N \, dp^N}{N! h^{3N}}. \tag{8}$$

Here F is a function of the particle number N, temperature T, and geometrical constraint X. Since the Hamiltonian $\mathcal{H}(q^N, p^N)$ is usually rotationally invariant, F is also rotationally invariant. Thus,

$$
\begin{aligned}
F(N, T, Y) &= F(N, T, JX) \\
&= F(N, T, RMX) \\
&= F(N, T, MX) \\
&= F(N, T, \sqrt{1 + 2\eta_X}\, X) \\
&= F(N, T, \eta_X, X),
\end{aligned}
\tag{9}
$$

i.e., F is a *function* of η_X, once X is chosen.

A function can always be expanded into Taylor series:

$$
\begin{aligned}
F(\eta_X, X) = F(0, X) &+ \left(\frac{\partial F}{\partial \eta_{ij}} \bigg|_{\eta_X = 0} \right) \eta_{ij} \\
&+ \frac{1}{2} \left(\frac{\partial^2 F}{\partial \eta_{ij} \partial \eta_{kl}} \bigg|_{\eta_X = 0} \right) \eta_{ij} \eta_{kl} + \dots
\end{aligned}
\tag{10}
$$

Because η_{ij} is symmetric, the expansion should only involve six independent variables: $\eta_{11}, \eta_{22}, \eta_{33}, \eta_{23}, \eta_{13}, \eta_{12}$. But that is often inconvenient for index contraction, so what people do is to symmetrize the expansion coefficients over η_{ij} and η_{ji} whenever possible, but pretending η_{ij}, η_{ji} to be different summation variables. Let us define second and fourth rank symmetrization operators:

$$
\hat{S}_2(G_{ij}) = \tfrac{1}{2}(G_{ij} + G_{ji}),
\tag{11}
$$

$$
\hat{S}_4(W_{ijkl}) = \tfrac{1}{4}(W_{ijkl} + W_{ijlk} + W_{jikl} + W_{jilk}).
\tag{12}
$$

The thermodynamic stress at configuration X is defined to be,

$$
t_{ij}(X) = \frac{1}{\Omega(X)} \hat{S}_2 \left(\frac{\partial F(\eta_X, X)}{\partial \eta_{ij}} \bigg|_{\eta_X = 0} \right),
\tag{13}
$$

and the elastic constant:

$$
C_{ijkl}(X) = \frac{1}{\Omega(X)} \hat{S}_4 \left(\frac{\partial^2 F(\eta_X, X)}{\partial \eta_{ij} \partial \eta_{kl}} \bigg|_{\eta_X = 0} \right),
\tag{14}
$$

where $\Omega(X)$ is the volume of the object at X, so t_{ij} and C_{ijkl} are intensive quantities. By definition,

$$
F(\eta_X, X) = F_0 + \Omega(X) \left\{ t_{ij}(X)\eta_{ij} + \tfrac{1}{2}C_{ijkl}(X)\eta_{ij}\eta_{kl} \right\} \dots
$$

$$
t_{ij} = t_{ji}, \quad C_{ijkl} = C_{ijlk} = C_{jikl} = C_{jilk}.
\tag{15}
$$

Notice that since t_{ij} and C_{ijkl} are expansion coefficients of η_X in $F(\eta_X, X)$ at $\eta_X = 0$, they themselves are not functions of η_X, but only of X. That means the definitions of thermodynamic stress and elastic constant do not require a reference state, since to evaluate them we use the object itself at that moment as the reference state. The use of this co-moving reference frame has some "strange" consequences, which is generally covered in differential geometry [48]. For instance,

$$t_{ij}(Y) \neq t_{ij}(X) + C_{ijkl}(X)(\eta_X^Y)_{kl} + \ldots, \tag{16}$$

which is not what one may expect for the Taylor expansion of the "first-order derivative" in terms of the "second-order derivative", which works when we use a fixed reference frame. In fact, in light of (5),

$$
\begin{aligned}
F(Z) &= F(\eta_Y^Z, Y) \\
&= F(Y) + \Omega(Y)\text{Tr}\left(t(Y)\eta_Y^Z\right) + \mathcal{O}\left((\eta_Y^Z)^2\right) \\
&= F(\eta_X^Z, X) \\
&= F(X) + \Omega(X)\text{Tr}\left(t(X)\eta_X^Z\right) + \frac{\Omega(X)}{2}\text{Tr}\left(\eta_X^Z \mathbf{C}(X)\eta_X^Z\right) \\
&\quad + \mathcal{O}\left((\eta_X^Z)^3\right)
\end{aligned}
\tag{17}
$$
$$\tag{18}$$

The linear coefficient of η_Y^Z in (17) and (18) must be equal. Plugging in (5) to (18), we have,

$$
\begin{aligned}
F(Z) &= \text{const} + \Omega(X)\text{Tr}\left(Jt(X)J^T \eta_Y^Z\right) + \Omega(X)\text{Tr}\left(J\eta_X^Y \mathbf{C}(X)J^T \eta_Y^Z\right) \\
&\quad + \mathcal{O}\left((\eta_X^Y)^2\right)\eta_Y^Z + \mathcal{O}\left((\eta_Y^Z)^2\right).
\end{aligned}
\tag{19}
$$

Therefore matching the linear coefficient of η_Y^Z to that of (17), we have,

$$t(Y) = \frac{Jt(X)J^T}{\det|J|} + \frac{J(\mathbf{C}(X)\eta_X^Y)J^T}{\det|J|} + \mathcal{O}\left((\eta_X^Y)^2\right). \tag{20}$$

It can be shown that if J is constrained to be symmetric, then

$$t_{ij}(Y) = t_{ij}(X) + B_{ijkl}(X)(\eta_X^Y)_{kl} + \mathcal{O}\left((\eta_X^Y)^2\right), \tag{21}$$

where $B_{ijkl}(X)$ is the elastic stiffness coefficient [47]:

$$
\begin{aligned}
B_{ijkl}(X) = C_{ijkl}(X) + \tfrac{1}{2}(&\delta_{ik}t_{jl}(X) + \delta_{jk}t_{il}(X) + \delta_{il}t_{jk}(X) \\
&+ \delta_{jl}t_{ik}(X) - 2\delta_{kl}t_{ij}(X)).
\end{aligned}
\tag{22}
$$

$B_{ijkl}(X)$ is equal to $C_{ijkl}(X)$ only when $t_{ij}(X) = 0$, therefore the use of elastic constant as the linear expansion coefficient of stress versus strain (both defined above) is only a valid practice at zero load.

It can be proven by minimizing the Gibbs free energy [47] that equilibrium is reached at X when $t_{ij}(X) = \tau_{ij}$. Thus the two quantities have identical values *at equilibrium*; however they have different connotations physically.

Atomistic expressions for the thermodynamic stress and elastic constants can be derived for the canonical ensemble [50–52]. The partition function for a deformed system is,

$$Z(X, M) = \int_{MX} \exp(-\beta\mathcal{H}(\tilde{q}^N, \tilde{p}^N))\frac{\mathrm{d}\tilde{q}^N \, \mathrm{d}\tilde{p}^N}{N!h^{3N}}, \tag{23}$$

where we assume,

$$\mathcal{H}(\tilde{q}^N, \tilde{p}^N) = \sum_{n=1}^{N} \frac{\tilde{\mathbf{p}}_n^T \cdot \tilde{\mathbf{p}}_n}{2m_n} + V(\tilde{\mathbf{q}}_1, \tilde{\mathbf{q}}_2, \ldots, \tilde{\mathbf{q}}_N). \tag{24}$$

Under a change of variables $\tilde{\mathbf{q}}_n \to \mathbf{q}_n, \tilde{\mathbf{p}}_n \to \mathbf{p}_n$:

$$\tilde{\mathbf{q}}_n \equiv M\mathbf{q}_n, \quad \tilde{\mathbf{p}}_n \equiv M^{-1}\mathbf{p}_n, \quad n = 1, \ldots, N, \tag{25}$$

the Hamiltonian can be written as,

$$\mathcal{H}(q^N, p^N) = \sum_{n=1}^{N} \frac{\mathbf{p}_n^T M^{-2}\mathbf{p}_n}{2m_n} + V(M\mathbf{q}_1, M\mathbf{q}_2, \ldots, M\mathbf{q}_N). \tag{26}$$

Using (4) and also,

$$M^{-2} = \frac{1}{1 + 2\eta_X} = 1 - 2\eta_X + 4\eta_X^2 + \ldots \tag{27}$$

the partition function can be written as:

$$Z(X, \eta_X) = \int_X \exp\left[-\beta\left\{\sum_{n=1}^{N} \frac{\mathbf{p}_n^T(1 - 2\eta_X + 4\eta_X^2)\mathbf{p}_n}{2m_n}\right.\right.$$
$$\left.\left. + V\left(\left(1 + \eta_X - \tfrac{1}{2}\eta_X^2\right)q^N\right)\right\}\right]\mathrm{d}q^N\mathrm{d}p^N, \tag{28}$$

where we threw away the $N!h^{3N}$ constant. Using index notation η_{ij} for matrix η_X:

$$\frac{\partial F}{\partial \eta_{ij}} = -\frac{1}{\beta Z} \cdot \frac{\partial Z}{\partial \eta_{ij}} = \frac{1}{Z}\int_X T_{ij} \exp(-\beta\mathcal{H})\mathrm{d}q^N \, \mathrm{d}p^N \tag{29}$$

where,

$$\mathcal{H}(q^N, p^N) \approx \sum_{n=1}^{N} \frac{\mathbf{p}_n^T (1 - 2\eta_X + 4\eta_X^2)\mathbf{p}_n}{2m_n} + V\left(\left(1 + \eta_X - \tfrac{1}{2}\eta_X^2\right)q^N\right),$$

(30)

and

$$T_{ij} = \frac{\partial \mathcal{H}}{\partial \eta_{ij}} = \sum_{n=1}^{N} \frac{p_i^n (-\delta_{jk} + 4\eta_{jk})p_k^n}{m_n} + (\delta_{ik} - \eta_{ik})q_k^n \nabla_j^n V((1 + \eta_X)q^N).$$

(31)

Setting η_X to zero, we get the atomistic formula for the thermodynamic stress:

$$t_{ij}(X) = \left\langle \frac{1}{\Omega(X)} \hat{S}_2 \left(\sum_{n=1}^{N} \frac{-p_i^n p_j^n}{m_n} + q_i^n \nabla_j^n V(q^N) \right) \right\rangle.$$

(32)

The $\langle \rangle$ means canonical ensemble average in the original configuration X.

One may wonder why the sum (32) does not always give 0 at $T = 0$, since $\nabla_j^n V(q^N) \equiv 0$ for bulk atoms at equilibrium. The answer is that if we were to compute the stress using (32) as it stands now, we must count those atoms on the surface, whose equilibrium conditions $F_j^n = \nabla_j^n V(q^N)$ in general require the presence of external force F_j^n, which is the force the wall exerts on the atom to keep it within X. Since in (32) those F^n's are weighted by q^n's, this surface contribution does *not* vanish in the thermodynamic limit ($N, \Omega \to \infty$), as the surface energy does, on a per volume basis.

On the other hand, it appeals to one's intuition that stress originates from the bulk, not from the surface, and is an intensive quantity. This can be seen in the following way: because $V(q^N)$ in general is the sum of *local interactions*, for instance $V(q^N) = \sum_{\{lmn\}} W(q_l, q_m, q_n)$, where W's are three-body local interactions. Due to translational symmetry: $W(q_l + \delta, q_m + \delta, q_n + \delta) = W(q_l, q_m, q_n)$, one must have $\nabla^l W + \nabla^m W + \nabla^n W \equiv 0$, so the contribution of this specific interaction to the total (32) sum can be rewritten as $(q_i^l - q_i^n)\nabla_j^l W + (q_i^m - q_i^n)\nabla_j^m W$, conceptualized as $\Delta F \cdot \Delta q$, i.e., force contribution weighted by the relative distance between action and reaction. Through this *localization* transform, all q^n weighting factors in the sum can be converted to Δq's which are no larger than the interatomic distance. In this transformed summation, which should be converted from (32) as soon as the interatomic potential model is known, the surface contribution would vanish in the thermodynamic limit on a per volume basis, like the surface energy. So for local interactions, we can prove that the stress is intensive and indeed may be thought of as originating from the bulk.

To get the atomistic formula for elastic constants, we need to further differentiate (29):

$$\frac{\partial^2 F}{\partial \eta_{ij}\, \partial \eta_{kl}} = \frac{1}{Z} \int\limits_X \left(\frac{\partial T_{ij}}{\partial \eta_{kl}} - \beta T_{ij} T_{kl} \right) \exp(-\beta \mathcal{H}) \mathrm{d}q^N\, \mathrm{d}p^N$$

$$+ \frac{\beta}{Z} \left(\int\limits_X T_{kl}\, \exp(-\beta \mathcal{H}) \mathrm{d}q^N\, \mathrm{d}p^N \right) \langle T_{ij} \rangle$$

$$= \beta \{ \langle T_{ij} \rangle \langle T_{kl} \rangle - \langle T_{ij} T_{kl} \rangle \} + \left\langle \frac{\partial T_{ij}}{\partial \eta_{kl}} \right\rangle. \tag{33}$$

From (31) we can get:

$$\left. \frac{\partial T_{ij}}{\partial \eta_{kl}} \right|_{\eta_X = 0} = \sum_{n=1}^{N} \frac{4 p_i^n p_k^n}{m_n} \delta_{jl} + \sum_{m,n=1}^{N} \left\{ q_k^m q_i^n \nabla_l^m \nabla_j^n V(q^N) - \delta_{il} q_k^n \nabla_j^n V(q^N) \right\}. \tag{34}$$

So we get the unsymmetrized form of elastic constants:

$$D_{ijkl} = \beta \Omega(X) \left(\langle t_{ij} \rangle \langle t_{kl} \rangle - \langle t_{ij} t_{kl} \rangle \right) + \frac{1}{\Omega(X)} \left\langle \sum_{n=1}^{N} \frac{4 p_i^n p_k^n}{m_n} \delta_{jl} \right\rangle$$

$$+ \frac{1}{\Omega(X)} \left\langle \sum_{m,n=1}^{N} q_k^m q_i^n \nabla_l^m \nabla_j^n V(q^N) - \sum_{n=1}^{N} q_k^n \nabla_j^n V(q^N) \delta_{il} \right\rangle. \tag{35}$$

The first term is defined to be the fluctuation term. The last term is defined to be the Born term, usually written as C_{ijkl}^B. The elastic constant is therefore

$$C_{ijkl} = \hat{S}_4(D_{ijkl}), \tag{36}$$

which is valid at finite temperature and for arbitrary stress. The summation (35) also needs to undergo the localization procedure as (32) to be computable in atomistic calculations.

Equations (32) and (35) are only applicable to canonical ensemble. For micro-canonical ensemble, a different set of formulas can be derived [53]. For more details, see Chap. 2.16.

2. Dislocation Core Energy

The dislocation core is a remarkable bond-cutting machine (the "sharpest knife") that nature comes up with to relieve the stored elastic energy. While the internal mechanisms of this machine can be highly complicated, the overall effect is that atomic bonds come into the machine, get cut in shear, and new

bonds with dislocated neighbors are left in the wake, much like a combine in a crop field. With its operation, diffuse elastic strain in the environment are collected and condensed into local inelastic (transformation) strain in a one-atomic-layer thin platelet, the glide plane [5].

There are actually two definitions of the dislocation core size [24, 25], a physical core width and a mathematical/elasticity core width. The physical core was described in the first paragraph, and is defined by atoms whose local atomic order like the coordination number or inversion symmetry (Chap. 2.31) is drastically different from that of the crystalline bulk, from which we may define a core size r_0^{phys}. In other words, the physical core is the set of atoms which are participating actively in the bond-cutting business. Obviously, r_0^{phys} is significant and useful, but needs not be a precise real number (like $1.8234a_0$) due to lattice discreteness. In contrast, the mathematical core radius r_0 and core energy E_{core} can be defined precisely as real numbers from an asymptotic expansion of the total energy of a dislocation dipole in an infinite, and otherwise perfect, atomic lattice,

$$E(\mathbf{d}) = 2E_{\text{core}} + 2A(\theta) + \frac{K_s|\mathbf{b}|^2}{2\pi} \log \frac{|\mathbf{d}|}{r_0} + \mathcal{O}\left(|\mathbf{d}|^{-1}\right), \tag{37}$$

at large $|\mathbf{d}|$. Here, $E(\mathbf{d})$ is defined to be the total energy increase in a thought experiment of an infinite lattice whose atoms displace according to the leading-order Stroh solution [55] $\mathbf{u}_G(\mathbf{x})$ at $|\mathbf{x} - \mathbf{d}/2|$, $|\mathbf{x} + \mathbf{d}/2| \gg r_0^{\text{phys}}$, but which are allowed to relax atomistically near the physical cores. As the Stroh solution is self-equilibrating (stress equilibrium is satisfied), the above thought experiment is well-posed and $E(\mathbf{d})$ is the final increase in the atomistic total energy. At large $|\mathbf{d}|$, the leading $\mathbf{d}$-dependent term in $E(\mathbf{d})$ must be $K_s|\mathbf{b}|^2 \log |\mathbf{d}|/2\pi$, with K_s proven invariant with respect to the displacement cut direction $\hat{\mathbf{d}} \equiv \mathbf{d}/|\mathbf{d}|$ [56]. Let us define θ to be the angle between $\hat{\mathbf{d}}$ and an arbitrarily chosen reference direction $\hat{\mathbf{a}}$, with $\hat{\mathbf{d}} \perp \xi$ and $\hat{\mathbf{a}} \perp \xi$, $|\hat{\mathbf{d}}|=|\hat{\mathbf{a}}|=1$, and ξ is the line direction of the straight dislocation. An asymptotic expansion of $E(\mathbf{d})$ at large $|\mathbf{d}|$ would yield $\mathcal{O}(\log |\mathbf{d}|)$, $\mathcal{O}(1)$, $\mathcal{O}(|\mathbf{d}|^{-1})$, ... terms. The $\mathcal{O}(1)$ term may contain a θ-dependent component $2A(\theta)$, and a θ-independent component. For the sake of definiteness, we require $A(\theta = 0) = 0$, and $\hat{\mathbf{a}}$ will be called the zero-angle reference axis. $A(\theta)$ is given entirely by anisotropic elasticity,

$$2A(\theta) = \sum_{\alpha=1}^{3} \frac{\mathbf{b}^T \mathbf{K}_\alpha \mathbf{b}}{4\pi} \log \frac{(\hat{d}_x + p_\alpha^r \hat{d}_y)^2 + (p_\alpha^i \hat{d}_y)^2}{(\hat{a}_x + p_\alpha^r \hat{a}_y)^2 + (p_\alpha^i \hat{a}_y)^2}, \tag{38}$$

where $p_\alpha \equiv p_\alpha^r + i p_\alpha^i$, $\alpha = 1..3$, are the three Stroh eigenvalues with nonnegative imaginary parts, and $\mathbf{K}_\alpha \equiv -2(\text{Re}(\mathbf{L}_\alpha)\text{Im}(\mathbf{L}_\alpha)^T + \text{Im}(\mathbf{L}_\alpha)\text{Re}(\mathbf{L}_\alpha)^T)$ is the mode-specific modulus [56], with $\sum_{\alpha=1}^{3} \mathbf{b}^T \mathbf{K}_\alpha \mathbf{b} = K_s|\mathbf{b}|^2$. Physically, $2A(\theta)$ is the rotational energy landscape of a dislocation dipole with fixed $|\mathbf{d}|$ in an infinite anisotropic medium [24], when $|\mathbf{d}|$ is asymptotically large. It is seen

from (38) that $A(\theta) = A(\theta + \pi)$. To illustrate, $A(\theta)$'s for Si $a_0/2[1\bar{1}0]$ and Mo $a_0/2[111]$ screw dislocations are evaluated and shown in Fig. 1.

With $\mathcal{O}(\log|\mathbf{d}|)$ and θ-dependent $\mathcal{O}(1)$ parts known, the $|\mathbf{d}|$- and θ-independent $\mathcal{O}(1)$ part of $E(\mathbf{d})$ can be used to determine the mathematical core r_0, E_{core} pair. Imagine for a fixed θ, we plot $E(\mathbf{d})$ data with $|\mathbf{d}|$ on a chart ($\mathbf{d}$ can only take discrete lattice spacing), and we would like to fit the data to a smooth function $\tilde{E}(\mathbf{d})$. We need to shift the function $K_s|\mathbf{b}|^2 \log|\mathbf{d}|/2\pi$ up or down to get a good fit at large $|\mathbf{d}|$. That shift operation is well defined asymptotically and is mathematically unique. If we ignore $|\mathbf{d}|^{-1}$, etc. terms in the fitting template $\tilde{E}(\mathbf{d}) \equiv 2E_{\text{core}} + 2A(\theta) + \frac{K_s|\mathbf{b}|^2}{2\pi} \log \frac{|\mathbf{d}|}{r_0}$, $2E_{\text{core}} + 2A(\theta)$ would be the abscissa of $\tilde{E}(\mathbf{d})$ at $|\mathbf{d}| = r_0$. It does *not* mean, however, that $E(r_0) = 2E_{\text{core}} + 2A(\theta)$, as $\tilde{E}(\mathbf{d})$ only fits $E(\mathbf{d})$ well at large $|\mathbf{d}|$ (satisfying at minimum $|\mathbf{d}| \gg 2r_0^{\text{phys}}$). It is thus clear that r_0, E_{core} are mathematical instruments to fit $E(\mathbf{d})$ to an asymptotic form and do not carry physical meaning in either quantity alone. If one likes, one may choose $r_0 = 1000|\mathbf{b}|$ and select E_{core} accordingly so $\tilde{E}(\mathbf{d})$ remains the same function and nothing is changed. There are several popular choices, however, such as (a) take $r_0 = |\mathbf{b}|$, (b) choose r_0 so $E_{\text{core}} = 0$, (c) $r_0 = r_0^{\text{phys}}$ to minimize confusion, (d) $r_0 = 1\text{Å}$ to simplify numerical calculation, etc. It is seen that except for (c), none of the r_0's has anything to do with a physical core size. It is also clear that although $\tilde{E}(\mathbf{d})$ by definition must fit $E(\mathbf{d})$ well at large $|\mathbf{d}|$, there should be a big error as $|\mathbf{d}| \to 2r_0^{\text{phys}}$ and the physical cores begin to overlap. Finally, r_0 and E_{core} (and $\hat{\mathbf{a}}$ too) combined
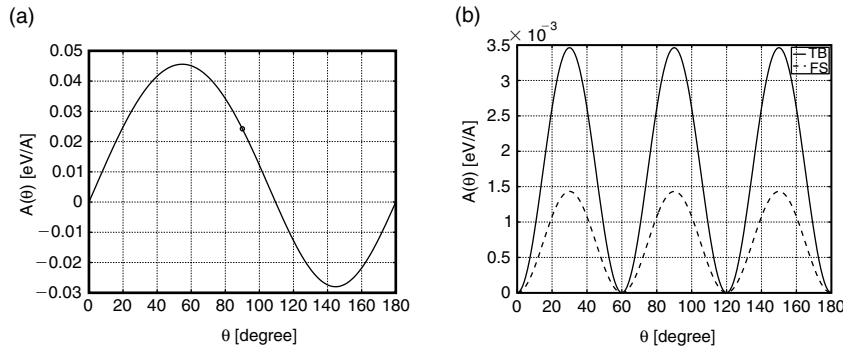
Figure 1. (a) The angular function $A(\theta)$ of $a_0/2[1\bar{1}0]$ shuffle-set screw dislocation in Stillinger–Weber potential Si [24], with $\langle11\bar{2}\rangle$ as the zero-angle reference axis $\hat{\mathbf{a}}$. The corresponding core energy is computed to be 0.502 eV/Å for $r_0 = |\mathbf{b}|$. In a separate calculation [54], with $\langle111\rangle$ as the zero-angle reference axis, the core energy was computed to be 0.526 eV/Å. The 0.024 eV/Å difference is verified to be exactly $A(\theta = \pi/2)$, as shown above in circle. (b) The angular function $A(\theta)$ for Mo $a_0/2$ [111] screw dislocation using the Finnis–Sinclair potential (dash line) and the tight-binding potential (solid line), both with $\hat{\mathbf{a}}$ chosen to be $\langle11\bar{2}\rangle$. There is $A(\theta) = A(\theta + \pi/3)$ due to crystal symmetry.

do carry physical meaning – as much as any other defect formation energies – for example in evaluating the absolute total energy of formation of a dislocation loop. The atomistically computed E_{core} is critical for constructing the total energy landscape of coarse-grained models like nodal dislocation dynamics.

From the above, it is apparent that the choice of the zero-angle reference axis $\hat{\mathbf{a}}$ influences the numerical value of E_{core}, in addition to the choice of r_0. This point is not widely appreciated. Indeed, even the existence of the dipole rotational energy $2A(\theta)$ has usually been ignored in the analyses of atomistic simulation results in the literature. Note from Eq. (38) that $A(\theta)$ originates entirely from elasticity. $A(\theta \neq n\pi)$ is generally non-zero for any dislocation dipole except screw dislocation dipole in isotropic medium. For example, $A(\theta)$ is non-zero for edge dislocation dipole in isotropic medium. E_{core} thoroughly characterizes the net energy consequence of core atomic relaxations, but one must be informed about what *elasticity function parameters* r_0 and $\hat{\mathbf{a}}$ are chosen as matching partners. For instance, it was reported [54] that E_{core} of $a_0/2[1\bar{1}0]$ shuffle-set screw dislocation in diamond cubic Si was $0.502 \, eV/Å$, with $r_0 = |\mathbf{b}|$ and using the Stillinger–Weber potential. Later, a separate, independent calculation gives $E_{core} = 0.526 \, eV/Å$ for the same setup. It is then traced back and determined that while the latter calculation uses definition $\hat{\mathbf{a}} = \langle 11\bar{2}\rangle$, the former calculation in effect used $\hat{\mathbf{a}} = \langle 111 \rangle$. The offset is exactly given by $A(\theta = \pi/2) = 0.024 \, eV/Å$ as shown in Fig. 1(a). So both calculations are correct, with the only difference in the choice of the zero-angle reference axis $\hat{\mathbf{a}}$ and a trivial conversion of E_{core}'s between them.

To reiterate, the numerical value of E_{core} carries no physical meaning unless $\hat{\mathbf{a}}$ and r_0 are specified. The conversion of E_{core} to other $\hat{\mathbf{a}}, r_0$ "basis" can be performed easily using the fact that $E(\mathbf{d})$ of Eq. (37), being a physical measurable in a well-posed thought experiment, is invariant, while $\hat{\mathbf{a}}, r_0, E_{core}$ are merely parameters in the mathematical representation of its asymptotic form. In the example next, we show how the core energy of BCC Mo screw dislocation can be calculated in a small supercells using the Finnis–Sinclair potential [57]. All our E_{core} values below will be based on $r_0 = |\mathbf{b}|$ and $\hat{\mathbf{a}} = \langle 11\bar{2}\rangle$. The setup is as follows. Define $\mathbf{e}_1 = a_0[11\bar{2}]$, $\mathbf{e}_2 = a_0[\bar{1}10]$, $\mathbf{e}_3 = a_0/2[111]$. An orthogonal supercell $7\mathbf{e}_1 \times 11\mathbf{e}_2 \times \mathbf{e}_3$ is almost square and contains 462 atoms, in which we can put in four equally spaced screw dislocations to form a quadrupole. Because of symmetry redundancy, this quadrupole cell can be mapped to an entirely equivalent dipole cell half its size with three edges $\mathbf{h}_1 = 7\mathbf{e}_1$, $\mathbf{h}_2 = 3.5\mathbf{e}_1 + 5.5\mathbf{e}_2 + 0.5\mathbf{e}_3$, $\mathbf{h}_3 = \mathbf{e}_3$. The $0.5\mathbf{e}_3$ in $\mathbf{h}_2$ is critical to this mapping, in view of the fact that $\epsilon_{total} = \epsilon_{elastic} + \epsilon_{plastic}$, where ϵ_{total} is total strain corresponding to the tilt of the supercell, $\epsilon_{plastic}$ is the plastic strain generated by the displacement cut in the dipole cell (in the quadrupole cell, $\epsilon_{plastic}$ is zero as there are two opposing cuts), and $\epsilon_{elastic}$ is the volume-averaged elastic strain in the supercell, which relates directly to the cell-averaged Virial stress τ_{virial}. So, by "preemptively" making $\epsilon_{total} = \epsilon_{plastic}$, we make sure that

the $\epsilon_{\text{elastic}} = 0$ and $\tau_{\text{virial}} \approx 0$. It can be shown that (a) $\tau_{\text{virial}} = 0$ minimizes the supercell total energy $E_{\text{atomistic}}$ with respect to cell shape $(\mathbf{h}_1, \mathbf{h}_2, \mathbf{h}_3)$ [24, 54], and (b) at dipole separation $\mathbf{d} = \mathbf{h}_1/2$, the local stresses at the first and second dislocations vanish simultaneously: $\tau_1 = \tau_2 = 0$. This stabilizes the two dislocations so they would not annihilate, which happens frequently in small supercell calculations. And even when they do not annihilate, a finite driving force would push the dislocation core against the lattice barrier and distort its shape from equilibrium, which introduces error to the computed core energy E_{core}.

We can now briefly discuss the image sum procedure for extracting the core energy from periodic supercell calculations. A detailed account is given in Chap. 2.21. An instructive approach to this problem is to think about how to explicitly construct a displacement field $\mathbf{u}(\mathbf{x})$ in the supercell, that (a) satisfies the displacement cut required by the dipole, (b) is self-equilibrating, and (c) is compatible with the PBC: $\mathbf{u}(\mathbf{x} + \mathbf{h}_i^0) = \mathbf{u}(\mathbf{x})$ and all orders of derivatives including the first, with $\{\mathbf{h}_i^0\}$ being the supercell edges before the dipole cut. The following Green's function sum

$$\tilde{\mathbf{u}}_\lambda(\mathbf{x}) \equiv \lambda \left(\mathbf{u}_{\text{G}}(\mathbf{x}) + \sum_{\mathbf{R} \neq 0} \mathbf{u}_{\text{G}}(\mathbf{x} - \mathbf{R}) \right) \tag{39}$$

could conceivably lead to $\mathbf{u}(\mathbf{x})$, where $\mathbf{u}_{\text{G}}(\mathbf{x})$ is the displacement field of an isolated dislocation dipole in an infinite medium (the one used in the thought experiment). The dislocation lines are all parallel to $\mathbf{h}_3^0$, and $\mathbf{R} = n_1 \mathbf{h}_1^0 + n_2 \mathbf{h}_2^0$, $n_1 = -N..N$, $n_2 = -\alpha N..\alpha N$. λ is from 0 to 1 to label the magnitude of the cut displacement from 0 to $\mathbf{b}$. Presence of the $\mathbf{u}_{\text{G}}(\mathbf{x})$ term in $\tilde{\mathbf{u}}_\lambda(\mathbf{x})$ will satisfy condition (a). Condition (b) is trivially satisfied as all Green's function displacements are self-equilibrating away from the cores. Condition (c) is a bit more subtle. But it can be rigorously shown that,

$$\tilde{\mathbf{u}}_\lambda(\mathbf{x} + \mathbf{h}_i^0) - \tilde{\mathbf{u}}_\lambda(\mathbf{x}) = \lambda \mathbf{D}(\alpha) \mathbf{h}_i^0 + \mathcal{O}\left(\frac{1}{N}\right) \tag{40}$$

as $N \to \infty$, where $\mathbf{D}(\alpha)$ is a 3×3 affine transformation matrix that depends on the image summation aspect ratio α only. $\mathbf{D}(\alpha)$ is the cause of the apparent conditional convergence. To get rid of it, we write:

$$\mathbf{u}_\lambda(\mathbf{x}) = \tilde{\mathbf{u}}_\lambda(\mathbf{x}) - \lambda \mathbf{D}(\alpha) \mathbf{x}. \tag{41}$$

It is seen now that $\mathbf{u}_\lambda(\mathbf{x})$ satisfies (a),(b),(c) simultaneously, so one can use $\mathbf{u}_{\lambda=1}(\mathbf{x})$ to transform atoms in the PBC cell without creating gaps or stress non-equilibrium. In practice, $\mathbf{D}(\alpha)$ is evaluated numerically by analyzing the behavior of $\tilde{\mathbf{u}}_\lambda(\mathbf{x})$ from image summations at a constant α and progressively large N's.

Suppose we start out with a PBC supercell $\{\mathbf{h}_i^0\}$ containing a stress-free crystal. We adiabatically change λ by effecting a cut increment $d\lambda \mathbf{b}$ along the

dipole cut in the cell. At each instant, the displacement field in the cell is $\mathbf{u}_\lambda(\mathbf{x})$, so the stress field $\sigma_\lambda(\mathbf{x})$ is available by plugging in $\nabla\mathbf{u}_\lambda(\mathbf{x})$. The incremental work is simply:

$$dW = d\lambda \int \mathbf{b} \cdot \sigma_\lambda(\mathbf{x}) \cdot \mathbf{n}\,dS, \tag{42}$$

which is converted to potential energy. Equations (39), (41), and (42) combined give a total energy expression that consists of:

- dipole self-energy in the form of (37)
- image dipole/displacement-cut coupling energy
- $\mathbf{D}(\alpha)$ stress/displacement-cut coupling energy

Summation over individual Stroh modes like Eq. (38) is needed to account for the dipole-dipole interaction energy $E_{\text{dipole}-\text{dipole}}$. The expression

$$E_{\text{dipole}-\text{dipole}} = \frac{K_s|\mathbf{b}|^2}{2\pi} \log \frac{|\mathbf{R}+\mathbf{d}||\mathbf{R}-\mathbf{d}|}{|\mathbf{R}|^2} \tag{43}$$

is simply incorrect in anisotropic medium as it ignores the $2A(\theta)$ angular-coupling terms. Note also that one needs to put in an extra factor of $1/2$:

$$\Delta W_{\text{image dipole}} = \tfrac{1}{2}E_{\text{dipole}-\text{dipole}} \tag{44}$$

for the $\mathbf{R}\neq 0$ dipole–dipole interaction energy, since one dipole "owns" only one half of the total coupling energy. All these follow automatically from Eq. (42).

The Eq. (41) setup is easier to explain, but gives a large supercell virial stress, as $\epsilon_{\text{total}} = 0$, and since

$$\epsilon_{\text{plastic}} \equiv \frac{\mathbf{D}_{\text{plastic}} + \mathbf{D}_{\text{plastic}}^T}{2}, \quad \mathbf{D}_{\text{plastic}} \equiv \frac{\mathbf{b}(\mathbf{d}\times\mathbf{h}_3^0)^T}{V},$$
$$\epsilon_{\text{elastic}} = -\epsilon_{\text{plastic}}. \tag{45}$$

Therefore in practice we use

$$\mathbf{u}_\lambda(\mathbf{x}) = \tilde{\mathbf{u}}_\lambda(\mathbf{x}) + \lambda(\mathbf{D}_{\text{plastic}} - \mathbf{D}(\alpha))\mathbf{x} \tag{46}$$

solution more often, with a new supercell $\mathbf{h}_i = \mathbf{h}_i^0 + \lambda\mathbf{D}_{\text{plastic}}\mathbf{h}_i^0$ that has been introduced for BCC Mo. The energy of this setup can be related to the previous one by accounting for the boundary work, which leads to a very simple result [24, 53].

To validate the above, we relax the Mo screw dislocation dipole in four supercell geometries using the Finnis–Sinclair potential:

i. $\mathbf{h}_1 = 7\mathbf{e}_1$, $\mathbf{h}_2 = 3.5\mathbf{e}_1 + 5.5\mathbf{e}_2 + 0.5\mathbf{e}_3$, $\mathbf{h}_3 = \mathbf{e}_3$ cell, containing 231 atoms,
ii. $\mathbf{h}_1 = 8\mathbf{e}_1$, $\mathbf{h}_2 = 16\mathbf{e}_2 + 0.5\mathbf{e}_3$, $\mathbf{h}_3 = \mathbf{e}_3$ cell, containing 768 atoms,

iii. $\mathbf{h}_1 = 16\mathbf{e}_1$, $\mathbf{h}_2 = 64\mathbf{e}_2 + 0.5\mathbf{e}_3$, $\mathbf{h}_3 = \mathbf{e}_3$ cell, containing 6, 144 atoms,
iv. $\mathbf{h}_1 = 32\mathbf{e}_1$, $\mathbf{h}_2 = 32\mathbf{e}_2 + 0.5\mathbf{e}_3$, $\mathbf{h}_3 = \mathbf{e}_3$ cell, containing 6, 144 atoms.

The differential displacement maps [58] of (i) and (ii) are shown in Fig. 2, in which the spontaneous polarities are manifest. If we use Å as the length unit, then we can write:

$$E_{\text{atom}} = E_{\text{elastic}} + 2 \left(E_{\text{core}} - \frac{K_s |\mathbf{b}|^2}{4\pi} \log r_0 \right) |\mathbf{h}_3^0|, \tag{47}$$

where E_{atom} is the increase in total energy in the PBC supercell, E_{elastic} is the result of the elastic energy summation without the r_0, E_{core} constants, and also by choosing $\hat{\mathbf{a}} = \langle 11\bar{2} \rangle$ so the $2A(\theta)$ term in Eq. (37) gives no contribution (but its equivalent anisotropic effects are present in the image dipole coupling energies). $K_s |\mathbf{b}|^2 / 4\pi$, the single dislocation energy prefactor, is 0.499 eV/Å for the Finnis–Sinclair potential. Numerical results for (i)–(iv) are shown in Table 1, respectively. We see that by varying the supercell size and shape, the elastic energy contribution E_{elastic} dominates the total energy landscape. However, the differences between E_{atom} and E_{elastic} remain remarkably constant. If we take $r_0 = |\mathbf{b}|$ and $\hat{\mathbf{a}} = \langle 11\bar{2} \rangle$, then $E_{\text{core}} = 0.300 \pm 0.001$ eV/Å,
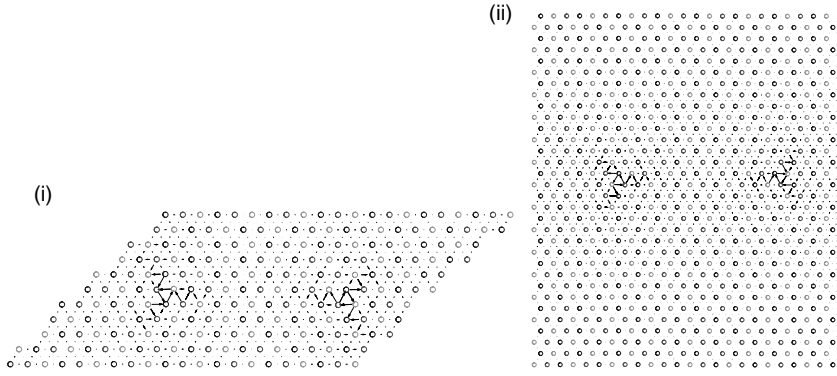
Figure 2. Differential displacement map [58] of Mo screw dislocation relaxed using the Finnis–Sinclair potential. (i) $\mathbf{h}_1 = 7\mathbf{e}_1$, $\mathbf{h}_2 = 3.5\mathbf{e}_1 + 5.5\mathbf{e}_2 + 0.5\mathbf{e}_3$, $\mathbf{h}_3 = \mathbf{e}_3$ cell. (ii) $\mathbf{h}_1 = 8\mathbf{e}_1$, $\mathbf{h}_2 = 16\mathbf{e}_2 + 0.5\mathbf{e}_3$, $\mathbf{h}_3 = \mathbf{e}_3$ cell.

Table 1. Mo screw dislocation core energy with $r_0 = |\mathbf{b}|$ and $\hat{\mathbf{a}} = \langle 11\bar{2} \rangle$ using the Finnis–Sinclair potential

	$E_{\text{supercell}}$ [eV]	E_{elastic} [eV]	E_{core} [eV/Å]
(i)	6.0410	7.1361	0.2995
(ii)	7.0069	8.0955	0.3006
(iii)	8.8935	9.9838	0.3003
(iv)	11.0432	12.1318	0.3007

a definitive result. Further, we note that cell (i), which contains only 231 atoms, is capable of representing the core energy very accurately.

3. Crack-tip Dislocation Emission

A stressed crack tip has two basic options to relieve its stored strain energy: surface creation by breaking bonds, or plastic deformation (localized shearing). Whichever route has the lower activation energy in the long run should be the dominant mechanism. Therefore activation energy calculations are essential for understanding brittle-to-ductile transitions (BDT). Dislocation nucleation [59, 60] and migration [61] are both possible rate-limiting step in BDT. The former has become one of the standard problems in nanomechanics [62, 63], because proper treatment of the crack and dislocation cores are necessary. Previous atomistic calculations focused on K_{emit}, the athermal dislocation emission threshold, and the so-called 2D activation pathway in which the dislocation is constrained to be always straight. Zhu *et al.* [2] have applied the nudged elastic band (NEB) method [36] to calculate the 3D bow-out nucleation pathway atomistically.

Figures 3a–3c show the calculation setup for Cu (111) crack using the empirical potential of Mishin [64]. The 3D minimum energy path (MEP) obtained at $K_{\mathrm{I}} = 0.44\,\mathrm{MPa}\sqrt{\mathrm{m}}$ is compared with 2D MEP in Fig. 3d. It is seen to be the lower pathway for the same initial and final states. The external load is applied via a fixed-displacement boundary condition for all the NEB nodes (i–ix) during path relaxation. We find that for this model of Cu with the unstable stacking energy $\gamma_{\mathrm{us}} = 158\,\mathrm{mJ/m^2}$, the Rice–Peierls model [62] underestimates both $K_{\mathrm{I,emit}}$ and the activation energy $Q(K_{\mathrm{I}})$ of partial dislocation emission. $K_{\mathrm{I,emit}}$ turns out to be $0.508\,\mathrm{MPa}\sqrt{\mathrm{m}}$, which is 45% greater than the $0.35\,\mathrm{MPa}\sqrt{\mathrm{m}}$ from the analytic formula [62]. Furthermore, at $(K_{\mathrm{I}}/K_{\mathrm{I,emit}})^2 = G_{\mathrm{I}}/G_{\mathrm{I,emit}} = 0.75$, we find $Q(K_{\mathrm{I}})$ to be 1.1 eV, which is significantly larger than the first continuum estimate of 0.18 eV based on a perturbative approach [62], and a second, improved estimate of 0.41 eV using a more flexible representation of the embryonic dislocation loop [63]. Preliminary analyses indicate that two factors may be causing the discrepancy, which if corrected, may lead to much better semi-continuum models. The first is the negligence of surface deformation energetics near the crack tip [59, 60]. The second is that we believe the continuum models may induce a systematic error in the dislocation core energy E_{core} (see last topic), which drives down the energy cost of nucleating a half loop. We suggest that whenever one uses semi-continuum models calculating activation energies, the core energies of straight dislocations should first be calibrated against atomistic results. The semi-continuum model may then be systematically improved to give better core energies, or if not, very often the error can be conveniently adsorbed in
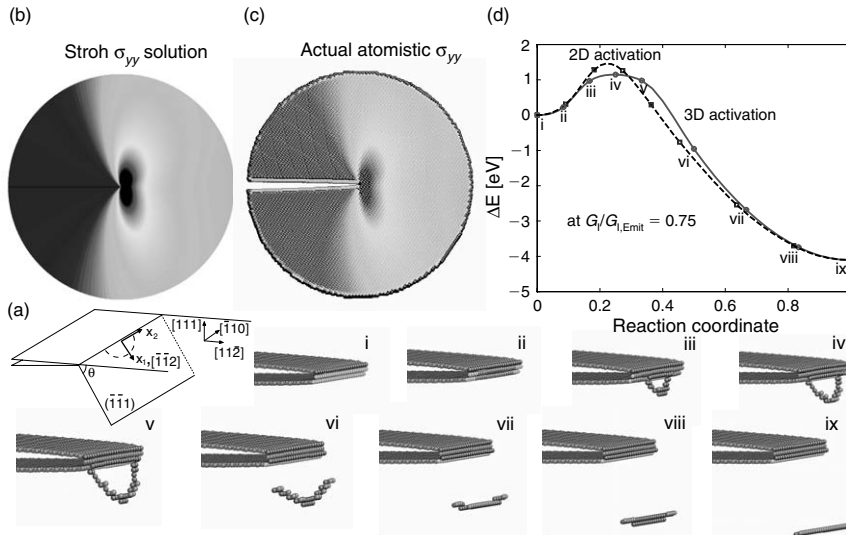
Figure 3. (a) Geometry of the mode-I crack [2], containing 24 unit cells (61 Å) in thickness (periodic boundary condition) and 103,920 Cu atoms in a $R = 80$ Å cylinder. Atoms within 5 Å of the cylinder border are fixed according to anisotropic linear elastic [65] solution. (b) Continuum Stroh solution and (c) the actual atomistic local stress distribution [20] of σ_{yy} at $G_I/G_{I,\text{emit}} = 0.75$. (d) 3D activation minimum energy path (solid line) of partial dislocation emission by bow-out, and its competing 2D pathway (dash line). i–ix show the sequential nine NEB nodes or images on the minimum energy path, with iv being the saddle point; atoms whose coordination number [66] differs from 12 are not shown. Note that a stacking fault is actually dragged behind the dislocation.

heuristic gradient functionals like $\kappa|\nabla\mathbf{u}_{\parallel}(\mathbf{x})|^2$. Otherwise the semi-continuum model calculating activation energies will have a systematic "core energy error" compared to atomistic results. This recommendation is quite general since heterogeneous nucleation of dislocation half loops by 3D bow-out is ubiquitous in cross-slip, slip transmission across grain and phase boundaries, initiation at surface asperities, etc. That the program has not been carried out before has more to do with the fact that the proper definition of dislocation core energy and numerically precise way to calculate it atomistically were only worked out recently [24, 25].

Figure 4 shows the saddle-point configuration obtained at $G_I/G_{I,\text{emit}} = 0.75$. It shows the birth of a shear-dominant singularity (embryonic dislocation loop) near a tensile-dominant singularity, the crack. To make connections with continuum models, we calculate the relative displacement between atoms on two sides of the slip plane. This completely discrete data set are then interpolated to form a continuum field estimate $\mathbf{u}(\mathbf{x})$, which is further decomposed into shear shock component $\mathbf{u}_{\parallel}(\mathbf{x})$ parallel to the slip plane (localized inelastic, or transformation, strain), and tensile opening component $\mathbf{u}_{\perp}(\mathbf{x})$ normal to
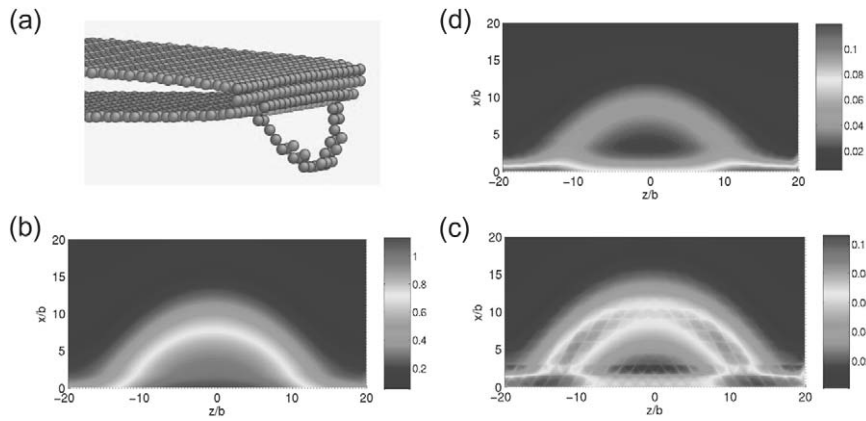
Figure 4. Analysis of the inelastic shock [5] displacement field $\mathbf{u}(\mathbf{x})$ on the inclined slip plane at the saddle point iv, obtained by 2D spline interpolation of the discrete atomic displacements. (a) Atomic view. (b) Shear component $\mathbf{u}_{\parallel}(\mathbf{x})$ normalized by $\mathbf{b}_p = a_0[112]/6$, and (c) $|\nabla\mathbf{u}_{\parallel}(\mathbf{x})|^2$. (d) Tensile opening component $\mathbf{u}_{\perp}(\mathbf{x})$ normalized by the interplanar spacing $h_0 = 3^{-1/2}a_0$.

the slip plane (large, but still elastic). The dislocation core is best visualized by looking at $|\nabla\mathbf{u}_{\parallel}(\mathbf{x})|^2$ (Fig. 4c), showing that the core is simply the domain wall between inelastically sheared and unsheared regions [5]. Yet, in the heart of this shear-dominant secondary singularity, there is also a little tensile component. Figure 4d shows that $\mathbf{u}_{\perp}(\mathbf{x})$ is maximized near where $|\nabla\mathbf{u}_{\parallel}(\mathbf{x})|^2$ is maximized. Such are the intricacies of shear-tension coupling, and one kind of singularity giving birth to the opposite kind. For instance, we know that when a lot of dislocations are piled up on a hard interface, a microcrack may also be nucleated heterogeneously.

References

[1] R. Phillips, *Crystals, Defects and Microstructures: Modeling Across Scales*, Cambridge University Press, Cambridge, 2001.

[2] T. Zhu, J. Li, and S. Yip, "Atomistic study of dislocation loop emission from a crack tip," *Phys. Rev. Lett.*, 93, 025503, 2004; T. Zhu, J. Li, and S. Yip, "Atomistic configurations and energetics of crack extension in silicon," *Phys. Rev. Lett.*, 93, 205504, 2004; T. Zhu, J. Li, K.J. Van Vliet, S. Ogata, S. Yip, and S. Suresh, "Predictive modeling of nanoindentation-induced homogeneous dislocation nucleation in copper," *J. Mech. Phys. Solids*, 52, 691–724, 2004.

[3] M. Allen and D. Tildesley, *Computer Simulation of Liquids*, Clarendon Press, New York, 1987.

[4] D. Frenkel and B. Smit, *Understanding Molecular Simulation: From Algorithms to Applications*, 2nd edn., Academic, San Diego, 2002.

[5] J. Li, A.H.W. Ngan, and P. Gumbsch, "Atomistic modeling of mechanical behavior," *Acta Mater.*, 51, 5711–5742, 2003.

[6] F.F. Abraham, R. Walkup, H.J. Gao, M. Duchaineau, T.D. De la Rubia, and M. Seager, "Simulating materials failure by using up to one billion atoms and the world's fastest computer: work-hardening," *Proc. Natl Acad. Sci. USA.*, 99, 5783–5787, 2002.

[7] J. Schiotz, F.D. Di Tolla, and K.W. Jacobsen, "Softening of nanocrystalline metals at very small grain sizes," *Nature*, 391, 561–563, 1998.

[8] V. Yamakov, D. Wolf, S.R. Phillpot, and H. Gleiter, "Dislocation–dislocation and dislocation–twin reactions in nanocrystalline Al by molecular dynamics simulation," *Acta Mater.*, 51, 4135–4147, 2003.

[9] J. Schiotz and K.W. Jacobsen, "A maximum in the strength of nanocrystalline copper," *Science*, 301, 1357–1359, 2003.

[10] V. Yamakov, D. Wolf, S.R. Phillpot, A.K. Mukherjee, and H. Gleiter, "Deformation-mechanism map for nanocrystalline metals by molecular-dynamics simulation," *Nat. Mater.*, 3, 43–47, 2004.

[11] H. Van Swygenhoven, P.M. Derlet, and A.G. Froseth, "Stacking fault energies and slip in nanocrystalline metals," *Nat. Mater.*, 3, 399–403, 2004.

[12] A.J. Haslam, V. Yamakov, D. Moldovan, D. Wolf, S.R. Phillpot, and H. Gleiter, "Effects of grain growth on grain-boundary diffusion creep by molecular-dynamics simulation," *Acta Mater.*, 52, 1971–1987, 2004.

[13] A. Hasnaoui, H. Van Swygenhoven, and P.M. Derlet, "Dimples on nanocrystalline fracture surfaces as evidence for shear plane formation," *Science*, 300, 1550–1552, 2003.

[14] A. Latapie and D. Farkas, "Molecular dynamics investigation of the fracture behavior of nanocrystalline alpha-Fe," *Phys. Rev. B*, 69, art. no.–134110, 2004.

[15] M.H. Muser, "Towards an atomistic understanding of solid friction by computer simulations," *Comput. Phys. Commun.*, 146, 54–62, 2002.

[16] M. Urbakh, J. Klafter, D. Gourdon, and J. Israelachvili, "The nonlinear nature of friction," *Nature*, 430, 525–528, 2004.

[17] C.L. Kelchner, S.J. Plimpton, and J.C. Hamilton, "Dislocation nucleation and defect structure during surface indentation," *Phys. Rev. B*, 58, 11085–11088, 1998.

[18] J.A. Zimmerman, C.L. Kelchner, P.A. Klein, J.C. Hamilton, and S.M. Foiles, "Surface step effects on nanoindentation," *Phys. Rev. Lett.*, 8716, art. no.–165507, 2001.

[19] G.S. Smith, E.B. Tadmor, N. Bernstein, and E. Kaxiras, "Multiscale simulations of silicon nanoindentation," *Acta Mater.*, 49, 4089–4101, 2001.

[20] K.J. Van Vliet, J. Li, T. Zhu, S. Yip, and S. Suresh, "Quantifying the early stages of plasticity through nanoscale experiments and simulations," *Phys. Rev. B*, 67, 2003.

[21] V. Vitek, "Core structure of screw dislocations in body-centred cubic metals: relation to symmetry and interatomic bonding," *Philos. Mag.*, 84, 415–428, 2004.

[22] H. Koizumi, Y. Kamimura, and T. Suzuki, "Core structure of a screw dislocation in a diamond-like structure," *Philos. Mag. A*, 80, 609–620, 2000.

[23] C. Woodward and S.I. Rao, "*Ab initio* simulation of (a/2) < 110] screw dislocations in gamma-TiAl," *Philos. Mag.*, 84, 401–413, 2004.

[24] W. Cai, V.V. Bulatob, J.P. Chang, J. Li, and S. Yip, "Periodic image effects in dislocation modelling," *Philos. Mag.*, 83, 539–567, 2003.

[25] J. Li, C.-Z. Wang, J.-P. Chang, W. Cai, V.V. Bulatov, K.-M. Ho, and S. Yip, "Core energy and Peierls stress of screw dislocation in bcc molybdenum: a periodic cell tight-binding study," *Phys. Rev. B*, 70, 104113, 2004.

[26] H.C. Huang, G.H. Gilmer, and T.D. de la Rubia, "An atomistic simulator for thin film deposition in three dimensions," *J. Appl. Phys.*, 84, 3636–3649, 1998.

[27] L. Dong, J. Schnitker, R.W. Smith, and D.J. Srolovitz, "Stress relaxation and misfit dislocation nucleation in the growth of misfitting films: molecular dynamics simulation study," *J. Appl. Phys.*, 83, 217–227, 1998.

[28] D. Holland and M. Marder, "Ideal brittle fracture of silicon studied with molecular dynamics," *Phys. Rev. Lett.*, 80, 746–749, 1998.

[29] M.J. Buehler, F.F. Abraham, and H.J. Gao, "Hyperelasticity governs dynamic fracture at a critical length scale," *Nature*, 426, 141–146, 2003.

[30] R. Perez and P. Gumbsch, "Directional anisotropy in the cleavage fracture of silicon," *Phys. Rev. Lett.*, 84, 5347–5350, 2000.

[31] N. Bernstein and D.W. Hess, "Lattice trapping barriers to brittle fracture," *Phys. Rev. Lett.*, 91, art. no.–025501, 2003.

[32] S.J. Zhou, D.M. Beazley, P.S. Lomdahl, and B.L. Holian, "Large-scale molecular dynamics simulations of three-dimensional ductile failure," *Phys. Rev. Lett.*, 78, 479–482, 1997.

[33] P. Keblinski, D. Wolf, S.R. Phillpot, and H. Gleiter, "Structure of grain boundaries in nanocrystalline palladium by molecular dynamics simulation," *Scr. Mater.*, 41, 631–636, 1999.

[34] M. Mrovec, T. Ochs, C. Elsasser, V. Vitek, D. Nguyen-Manh, and D.G. Pettifor, "Never ending saga of a simple boundary," *Z. Metallk.*, 94, 244–249, 2003.

[35] M.L. Falk and J.S. Langer, "Dynamics of viscoplastic deformation in amorphous solids," *Phys. Rev. E*, 57, 7192–7205, 1998.

[36] G. Henkelman and H. Jonsson,"Improved tangent estimate in the nudged elastic band method for finding minimum energy paths and saddle points," *J. Chem. Phys.*, 113, 9978–9985, 2000.

[37] T. Vegge and W. Jacobsen, "Atomistic simulations of dislocation processes in copper," *J. Phys.-Condes. Matter*, 14, 2929–2956, 2002.

[38] V.V. Bulatov, S. Yip, and A.S. Argon, "Atomic modes of dislocation mobility in silicon," *Philos. Mag. A*, 72, 453–496, 1995.

[39] M. Wen and A.H.W. Ngan, "Atomistic simulation of kink-pairs of screw dislocations in body-centred cubic iron," *Acta Mater.*, 48, 4255–4265, 2000.

[40] B.D. Wirth, G.R. Odette, D. Maroudas, and G.E. Lucas, "Energetics of formation and migration of self-interstitials and self-interstitial clusters in alpha-iron," *J. Nucl. Mater.*, 244, 185–194, 1997.

[41] T.D. de la Rubia, H.M. Zbib, T.A. Khraishi, B.D. Wirth, M. Victoria, and M.J. Caturia, "Multiscale modelling of plastic flow localization in irradiated materials," *Nature*, 406, 871–874, 2000.

[42] R. Devanathan, W.J. Weber, and F. Gao, "Atomic scale simulation of defect production in irradiated 3CSiC," *J. Appl. Phys.*, 90, 2303–2309, 2001.

[43] E.B. Tadmor, M. Ortiz, and R. Phillips, "Quasicontinuum analysis of defects in solids," *Philos. Mag. A*, 73, 1529–1563, 1996.

[44] V. Bulatov, F.F. Abraham, L. Kubin, B. Devincre, and S. Yip, "Connecting atomistic and mesoscale simulations of crystal plasticity," *Nature*, 391, 669–672, 1998.

[45] V.B. Shenoy, R. Miller, E.B. Tadmor, D. Rodney, R. Phillips, and M. Ortiz, "An adaptive finite element approach to atomic-scale mechanics – the quasicontinuum method," *J. Mech. Phys. Solids*, 47, 611–642, 1999.

[46] R. Madec, B. Devincre, L. Kubin, T. Hoc, and D. Rodney, "The role of collinear interaction in dislocation-induced hardening," *Science*, 301, 1879–1882, 2003.

[47] J.H. Wang, J. Li, S. Yip, S. Phillpot, and D. Wolf, "Mechanical instabilities of homogeneous crystals," *Phys. Rev. B*, 52, 12627–12635, 1995.

[48] I.S. Sokolnikoff, *Tensor Analysis, Theory and Applications to Geometry and Mechanics of Continua.*, 2nd edn., Wiley, New York, 1964.

[49] S.C. Hunter, *Mechanics of Continuous Media*, 2nd edn., E. Horwood, Chichester, 1983.

[50] J.F. Lutsko, "Stress and elastic-constants in anisotropic solids – molecular dynamics techniques," *J. Appl. Phys.*, 64, 1152–1154, 1988.

[51] J.F. Lutsko, "Generalized expressions for the calculation of elastic constants by computer-simulation," *J. Appl. Phys.*, 65, 2991–2997, 1989.

[52] J.R. Ray, "Elastic-constants and statistical ensembles in molecular dynamics," *Comput. Phys. Rep.*, 8, 111–151, 1988.

[53] T. Cagin and J.R. Ray, "Elastic-constants of sodium from molecular-dynamics," *Phys. Rev. B*, 37, 699–705, 1988.

[54] W. Cai, V.V. Bulatov, J.P. Chang, J. Li, and S. Yip, "Anisotropic elastic interactions of a periodic dislocation array," *Phys. Rev. Lett.*, 86, 5727–5730, 2001.

[55] A. Stroh, "Steady state problems in anisotropic elasticity," *J. Math. Phys.*, 41, 77–103, 1962.

[56] J. Hirth and J. Lothe, *Theory of Dislocations*, 2nd edn., Wiley, New York, 1982.

[57] M.W. Finnis and J.E. Sinclair, "A simple empirical *n*-body potential for transition-metals," *Philos. Mag. A*, 50, 45–55, 1984.

[58] V. Vitek, "Theory of core structures of dislocations in body-centered cubic metals," *Cryst Lattice Defects*, 5, 1–34, 1974.

[59] J. Knap and K. Sieradzki, "Crack tip dislocation nucleation in FCC solids," *Phys. Rev. Lett.*, 82, 1700–1703, 1999.

[60] J. Schiotz and A.E. Carlsson, "The influence of surface stress on dislocation emission from sharp and blunt cracks in fcc metals," *Philos. Mag. A*, 80, 69–82, 2000.

[61] P. Gumbsch, J. Riedle, A. Hartmaier, and H.F. Fischmeister, "Controlling factors for the brittle-to-ductile transition in tungsten single crystals," *Science*, 282, 1293–1295, 1998.

[62] J.R. Rice and G.E. Beltz, "The activation-energy for dislocation nucleation at a crack," *J. Mech. Phys. Solids*, 42, 333–360, 1994.

[63] G. Xu, A.S. Argon, and M. Oritz, "Critical configurations for dislocation nucleation from crack tips," *Philos. Mag. A*, 75, 341–367, 1997.

[64] Y. Mishin, M.J. Mehl, D.A. Papaconstantopoulos, A.F. Voter, and J.D. Kress, "Structural stability and lattice defects in copper: *ab initio*, tight-binding, and embedded-atom calculations," *Phys. Rev. B*, 6322, art. no.–224106, 2001.

[65] A. Stroh, "Dislocations and cracks in anisotropic elasticity," *Phil. Mag.*, 7, 625, 1958.

[66] J. Li, "Atomeye: an efficient atomistic configuration viewer," *Model. Simul. Mater. Sci. Eng.*, 11, 173–177, 2003.